Chapter 10

Shape-Controlled Synthesis of Metal Oxide Nanocrystals

Cao Thang Dinh,[a] Thanh Dinh Nguyen,[a] Freddy Kleitz,[b,*] and Trong On Do[a,*]

[a]*Department of Chemical Engineering, Laval University, Quebec, G1V 0A6, Canada*
[b]*Department of Chemistry, Laval University, Quebec, G1V 0A6, Canada*
*Trong-On.Do@gch.ulaval.ca, Freddy.Kleitz@chm.ulaval.ca

Inorganic nanoparticles (NPs) with well-defined geometries exhibiting unique size- and shape-dependent phenomena are of huge interest for a wide range of applications. Among all the functional materials designed at the nanoscale, metal oxides and mixed metal oxides are particularly attractive candidates from a scientific as well as technological point of view. The unique characteristics of metal oxides structured at the nanoscale make them the most diverse class of materials, with properties covering almost all of the aspects of materials science and solid state physics.

Given that new metal oxide nanomaterials are reported almost on a daily basis, considerable synthetic developments, for scalable and morphological control of metal oxide nanoparticles, remain to be done to fully exploit this family of compounds for further innovative nano-applications.

Controlled Nanofabrications: Advances and Applications
Edited by Ru-Shi Lui

ISBN 978-981-4316-87-3 (Hardback), 978-981-4364-51-5 (eBook)
www.panstanford.com

In this chapter, we review the synthetic methods that have so far been developed for the preparation of metal oxide nanoparticles, which include solvothermal/hydrothermal approaches, two-phase routes, microemulsions, and thermal decomposition methods. In addition, some current strategies for the shape control of metal oxide nanocrystals (NCs) encompassing oriented attachment, surface energy adjustment and selective adhesion, control of growth regime, and doping-induced shape evolution will also be reviewed. Finally, some future trends and perspectives in these research areas will also be outlined.

10.1 Introduction

Nanoparticles (particles of 1–100 nm in diameter) exhibit unique electronic, optical, photonic, and catalytic properties and have an ideal size for use as nanotechnological building blocks [1]. They may be composed of all sorts of substances, including metals, semiconductors, non-metal (e.g., C), organometallics, core–shell composite architectures, hybrid nanocrystals, and organic polymers. These particles often display properties intermediate between properties of atoms or molecules and those of condensed bulk matter because of their specific size and high surface-to-volume ratios. The properties of nanoparticles are drastically altered by change of size and shape, making them ideal candidates for applications in catalysis, nanoelectronics, sensing, optics, solar cells, medical diagnostics, drug delivery, cellular signaling, nanomedicine, and so forth [2–5].

Among all the functional materials to be synthesized at the nanoscale, metal oxides are particularly attractive, from a scientific as well as from a technological point of view. The unique characteristics of metal oxides make them the most diverse class of materials, with their properties encompassing almost all aspects of materials science and solid state physics [3]. The metal elements can form a large diversity of binary and mixed-oxide compounds, stoechiometric or non-stoechiometric. These elements can adopt many structural geometries with an electronic structure that can exhibit metallic (RuO_2, ReO_3), semiconductor (TiO_2, ZnO), or insulator ($BaTiO_3$) character. This exceptionally broad range of properties makes metal oxides a vital constituent in technological developments such as in the fabrication of microelectronic circuits, sensors, piezoelectric

devices, fuel cells, coatings for the passivation of surfaces against corrosion, purification devices, as additives in skin care products, and as catalysts. For example, almost all catalysts used in industrial applications involve an oxide as active phase, promoter, or "support." In the chemical and petrochemical industries, products worth billions of dollars are generated every year through processes that use oxide and metal/oxide catalysts. For the control of environmental pollution, catalysts or sorbents that contain oxides are employed to remove the CO, NO_x, and SO_x species formed during the combustion of fossil-derived fuels. Furthermore, some of the most active areas of the semiconductor industry involve the use of oxides. Thus, most of the chips used in computers contain an oxide component [7].

The syntheses of nanoparticles are generally grouped into two broad categories: "bottom up" and "top down" [8]. The process in which materials prepared from atomic precursors assemble to form clusters and subsequently nanoparticles is referred to as "bottom up" approach. Conversely, when the nanoscale is reached by physically disassembling large building blocks, the process is referred to as "top down" approach. The advantage of the physical methods is the possibility to produce a large quantity of nanoparticles, whereas the synthesis of uniform-sized nanoparticles and the control of their size remain very difficult by using the top-down route. The "Bottom up" approach is of primary interest for chemistry and materials science because the fundamental building blocks are atoms; thus colloidal chemical synthetic methods can be utilized to prepare uniform nanocrystals with controlled particle size. In the following, we will concentrate on solution phase synthetic methods that enable a proper shape and size control of metal oxide nanocrystals, methods which include solvothermal/hydrothermal procedures, two-phase routes, microemulsions, and thermal decomposition. These techniques involve the use of surfactant molecules and, consequently, result in oxide nanocrystals comprising an inorganic core coated with a layer of organic ligand molecules. This organic capping provides electronic and chemical passivation of the surface dangling bonds, prevents uncontrolled growth and agglomeration of the nanoparticles, and permits chemical manipulations of the nanoparticles similarly to large molecules having their solubility and reactivity determined by the nature of the surface ligands [9].

The shape of nanocrystals is crucial for the determination of their properties [10, 11]. The shape of nanocrystals can be classified

according to their dimensionality, such as zero dimensional (0D) for isotropic spheres, cubes, and polyhedrons; 1D for nanorods and nanowires; and 2D for thin films, discs, prisms, and platelets. The shape of the nanocrystals can be controlled by adjusting a number of thermodynamic (e.g., relative stability of crystal polymorphs) and kinetic (e.g., diffusion of reactants, surface adhesion of surfactants) factors. In this chapter, emphasis will be put on four major strategies for the shape control of metal oxide nanocrystals encompassing oriented attachment, surface energy and selective adhesion, control of growth regime, and doping-induced shape evolution.

10.2 Synthesis of Metal Oxide Nanocrystals

There are two main techniques by which all nanomaterials and metal oxide nanoparticles in particular can be synthesized: the physical, or top-down, approach, and the chemical, or bottom-up, approach. In the top-down approach one starts from a bulk material and attempts to break it down into nanoscale objects through physical methods. Bottom-up approach refers to the buildup of a structure from the bottom, i.e., atom-by-atom, molecule-by-molecule, or cluster-by-cluster, growing from a solution. This technique has been attractive for researchers, primarily because of the simplicity with which experiments can be conducted in the laboratory. Scaling the process to production of industrial-scale quantities of powders is, however, not as straightforward. A major advantage of solution processing is the ability to generate encapsulated nanoparticles by utilizing surfactants as protective shell, leading to very homogeneous and well-dispersed nanoparticles [12]. Surfactants are amphiphilic molecules composed of a polar head group and one or more hydrocarbon chains with hydrophobic character. The most commonly used ones in colloidal syntheses include alkyl- thiols, long chain amines, carboxylic and phosphonic acids, phosphine oxides, phosphine, phosphates, phosphonates, and various coordinating (e.g., ethers, THF, DMF) or non-coordinating solvents (e.g., alkanes, alkenes).

Surfactant-assisted synthetic methods provide convenient and efficient pathway for a reproducible and controlled synthesis of nanocrystals, and this not only because such methods allow for the metal oxide and mixed oxide nanocrystals to be precisely adjusted in terms of their size, shape, composition, and phase

structure at the nanoscale but also because these methods permit chemical hybridization with other functional materials for potential applications [14]. In general, nanocrystals obtained by the surfactant-assisted route exhibit excellent crystallinity and monodispersity in shape and size. Due to the rather strong bond between organic surfactants and oxides, it was proposed that these surfactants could change surface free energy and thus could influence the growth rates of specific crystal faces. These routes have generally the advantage of versatility compared to the surfactant-free routes, since in the absence of surfactants, control of the morphology through wet-chemical synthesis methods becomes more difficult. In the last decades, much research was dedicated on developing varieties of synthetic approaches, including multi-phase hydrothermal synthesis, solvothermal methods, microemulsion-base approaches, and thermal decomposition, in order to control at the nanoscale the size and shape of monodisperse metal oxide and mixed metal oxide crystals. In the following sections, we briefly present some representative chemical methods that have been developed so far for *shape-and-size-controlled* synthesis of metal oxide nanocrystals.

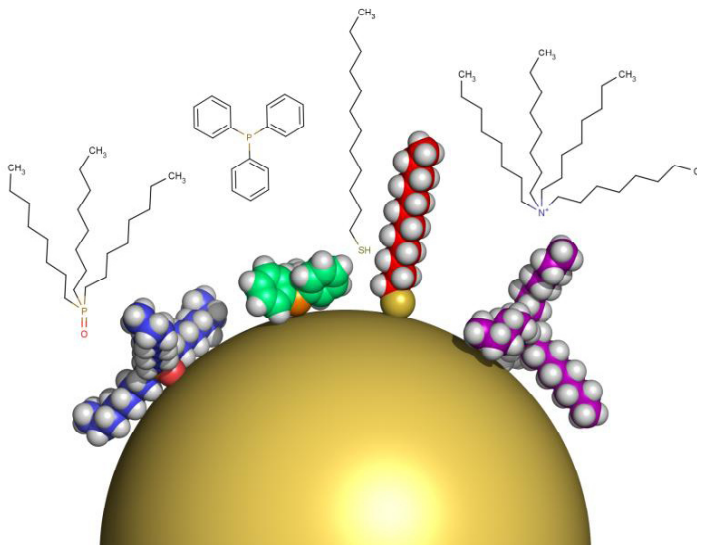

Figure 10.1 A nanoparticle of 5 nm core diameter with different hydrophobic ligand molecules. Left to right: Trioctylphosphine oxide, triphenylphosphine, dodecanethiol, and tetraoctylammonium bromide [13].

10.2.1 Hydrothermal/Solvothermal Methods

The solvothermal method provides a means of using solvents at temperatures well above their boiling points, by carrying out the reaction in a sealed vessel (bomb, autoclave). The pressure generated in the vessel caused by the solvent vapors (autogeneous pressure) elevates the boiling point of the solvent and often produces highly crystalline materials [15]. Mild solvothermal synthesis (<200°C) has been used to prepare ultrafine and phase-pure nanocrystalline products. Herein, we focus on the nonhydrolytic colloidal method that was utilized for the synthesis and design of a broad range of nanostructured materials with various geometrical motifs.

In the past years, several attempts had been made toward the controllable synthesis of various nanocrystals. For example, Li *et al.* [16–18] reported a facile solvothermal route to obtain II–VI group semiconductor nanocrystals, including CdE (E = S, Se, Te) and ZnE (E = S, Se). Short-chain alkylamines such as ethylenediamine were used as structure-directing coordination molecular species, which have been proven responsible for the specific morphologies of products. The authors also solvothermally synthesized size-controllable monodisperse PbSe and PbSe/PbS nanocrystals using lead acetate and Se powders [19]. De *et al.* [20] similarly synthesized cadmium-based nanostructures using cadmium nitrate and ethanol as precursor and solvent. Single-crystalline CdO micro-octahedron, polycrystalline CdO nanowires, and $Cd(OH)_2$ nanorods were obtained by only varying the amount of NaOH and the reaction temperature. Electrical resistivity measurement revealed semiconducting behavior of the CdO nanocrystal sample, owing to the presence of oxygen vacancies or excess metal interstitial atoms. Fu *et al.* [21] reported the phase-controlled synthesis of indium-based nanocrystals by using solvothermal reaction medium containing indium nitrate and a binary solution of water and *N,N*-dimethylformamide. The composition of the products can be modulated from cubic $In(OH)_3$ to orthorhombic InOOH and finally to cubic In_2O_3 structure by adjusting the amount of water. The Niederberger group [22] developed a nonaqueous sol-gel approach for the synthesis of a variety of oxide nanocrystals involving solvothermal treatment of metallic alkoxide precursors in benzyl alcohol solvent. TEM images shown in Fig. 10.2 display various kinds of nanocrystals with different shapes obtained by this method. The authors also demonstrated that the formation of

nanocrystals occurred through a nucleophilic mechanism between the precursor molecule and benzyl alcohol. As the presence in the final oxides obtained via these routes of halide impurities may be a drawback, alternative halide-free methods were developed as well. Thus, anatase nanoparticles of 5–20 nm in size were prepared through reaction of titanium tetra-isopropoxide with aldehydes and ketones under solvothermal conditions [23]. Other halide-free methods were developed by heating varieties of metal alkoxides, metal acetate, or metal acetylacetonates in the presence of benzyl alcohol in an autoclave at 200–250°C, leading to different oxide nanocrystals [24–27].

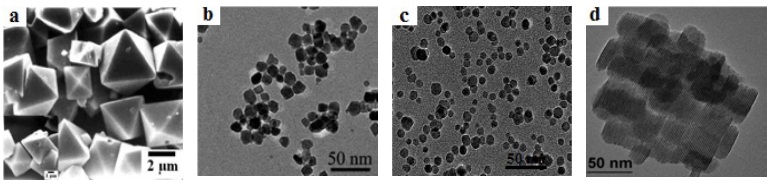

Figure 10.2 SEM image of (a) CdO nanooctahedrons [20]; and TEM images of (b) In_2O_3, (c) Fe_2O_3, and (d) Nd_2O_3 nanocrystals [24].

Recently, a modified solvothermal method for multigram scale synthesis of uniform vanadium oxide NCs was also reported using vanadium(V) diperoxo alkylammonium complexes in toluene or toluene/water medium in the presence of capping agents (e.g., aliphatic amines) [28]. The V(V) diperoxo tetraoctylammonium complexes, $VO(O_2)_2(TOA)$, were prepared from the two-phase system consisting of the V(V) diperoxo aqueous solution and tetraoctylammoniumligands (TOA^+) in toluene. Monodisperse vanadium oxide NCs with different sizes and shapes, including nanospheres, nanocubes, nanorices, and nanorods can be achieved by tuning of various reaction parameters, such as water content, types of V(V) diperoxo alkylammonium complexes, and alkyl chain length of the capping agents. For example, by increasing the water content in the reaction mixture, the shape evolved from nanospheres into nanorods. Figure 10.3 shows representative TEM images of these samples synthesized using the water/toluene ratio (W/T) of 0:40 to 2:40, 8:40, and 20:40. This data suggest that particle size and shape can easily be controlled by the water content in the reaction mixture under these synthesis conditions.

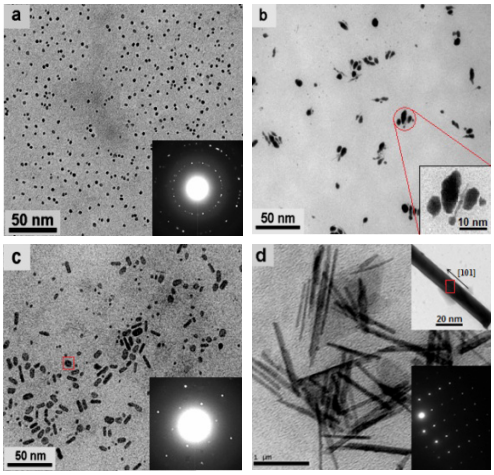

Figure 10.3 TEM images and corresponding SAED patterns of the as-made VO_2 nanocrystals synthesized from V(V) diperoxo tetraoctylammonium complexes in oleylamine at 180°C for 5 h with various water/toluene solvent ratios in volume (W/T): (a) W/T = 0:40, (b) W/T = 2:40, (c) W/T = 8:40, and (d) W/T = 20:40 [28].

The solvothermal method has also been applied to synthesize TiO_2 nanocrystals exhibiting various shapes [29, 30]. For example, TiO_2 nanoparticles and nanorods could be obtained by solvothermal reaction of titanium butoxide, linoleic acid, triethylamine, and cyclohexane as reported by Li *et al.* [29]. The decomposition of NH_4HCO_3 that provided H_2O for the hydrolysis reaction was found to be an important factor contributing to shape evolution of the particles. In the presence of NH_4HCO_3, the fast hydrolysis of the precursors with the water leads to the formation of nanoparticles. In contrast, in the absence of NH_4HCO_3, the slow nonhydrolytic condensation of precursors produces titania nanorods with uniform diameters of 3.3 nm and a length of up to 25 nm. TiO_2 nanowires could also be produced by solvothermal treatment of a mixture containing titanium tetroisopropoxide, ethylenediamine, and ethylene glycol (EG). The diameter of the nanowires was tailored by changing the amount of ethylenediamine [30]. TiO_2 nanocrystals with well-controlled shapes have been recently prepared by an interesting method based on solvothermal technique using both acid oleic acid (OA) and oleylamine (OM) as two capping surfactants,

and water vapor as the hydrolysing agent [31]. It was demonstrated that the presence of water vapor, in addition to a desired OA:OM molar ratio, plays a vital role in controlling size and shape of the TiO_2 nanocrystals.

The solvothermal method has also been extended to synthesize mixed metal oxide nanocrystals. For example, Yu *et al.* [32] described an effective EG-assisted solvothermal method to synthesize hierarchical $FeWO_4$ microcrystals using $FeCl_3{\cdot}6H_2O$ and $Na_2WO_4{\cdot}2H_2O$ as the precursors. It was found that the organic solvent EG had a critical role both as a reducing agent and as a structure-directing agent in driving such architectures by an oriented attachment of primary nanoparticles. Moreover, a certain amount of CH_3COONa was necessary for the formation of these unique $FeWO_4$ microstructures. The Li group [33] has successfully prepared under solvothermal condition series of novel hollow CeO_2–ZrO_2 nanocage materials with controlled shapes, sizes, and compositions, by adding zirconium(IV) into a glycol solution containing CeO_2 nanospheres (Fig. 10.4). The formation of cage-structured CeO_2–ZrO_2 nanomaterials was explained on the basis of the Kirkendall effect. Namely, when Zr^{4+} ions were added into the system, they diffused readily into ceria forming a solid solution of the type $Ce_{1-x}Zr_xO_2$. Meanwhile, the diffusion rate of the special secondary nanostructure of the resulting clusters was obviously much faster than that of the single-element nanostructure, leading to the favored formation of hollow nanostructures of the $Ce_{1-x}Zr_xO_2$ type.

Rare earth orthovanadate crystals have potential applications as catalysts and support, owing to their high surface area, thermal stability, and oxygen storage/release capacity (OSC) [34–36]. Recently, a novel and reproducible solvothermal method was developed for the synthesis of monodisperse $SmVO_4$ and $CeVO_4$ nanocrystals [37]. Metal nitrates and bulk metal oxide powders were usual precursors due to their commercial availability and their relatively low cost. The shape of $SmVO_4$ and $CeVO_4$ NCs could be controlled by tuning of the synthesis temperature.

TEM images of the samples synthesized under these solvothermal conditions at 150 and 180°C for 16 h are shown in Fig. 10.5. The transformation of both cubic-shaped $SmVO_4$ and round-shaped $CeVO_4$ NCs into uniform nanospheres, while preserving the particle size, by increasing synthesis temperature from 150 to 180°C could be explained by the Wuff facets theory [38].

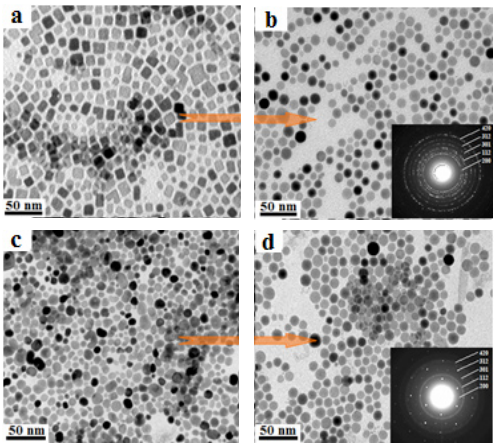

Figure 10.4 TEM images of (a) nearly monodisperse spherical ceria nanocrystals, (b) the corresponding $Ce_{1-x}Zr_xO_2$ nanocages, (c) cubic-like ceria nanocrystals, and (d) the corresponding $Ce_{1-x}Zr_xO_2$ nanocages [33].

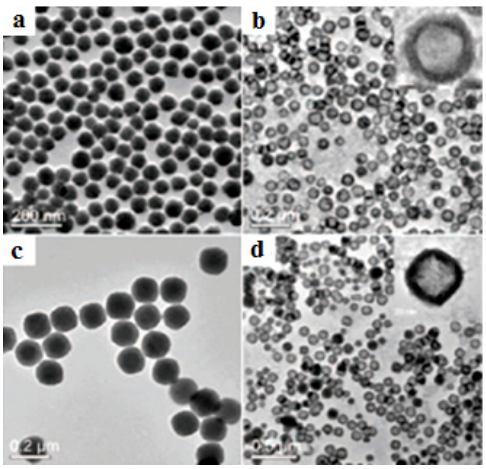

Figure 10.5 TEM images of 15 nm-sized $ReVO_4$ nanocrystals synthesized at different reaction tempe ratures: (a) $SmVO_4$ nanocubes, 150°C; (b) $SmVO_4$ nanocubes, 180°C; (c) $CeVO_4$ nanocubes, 150°C; and (d) $CeVO_4$ nanocubes, 180°C [37].

Pure rare earth oxide nanocrystals could also be obtained using solvothermal route. Nguyen *et al.* [39] reported the synthesis of the micro- and nanostructures of monoclinic ErOOH and cubic Er_2O_3 particles with different size and shapes by hydro-solvothermal

reaction using erbium nitrate and decanoic acid as precursor and capping agent, respectively, in a water–ethanol medium at 120–180°C for 24 h. After the synthesis reaction, the nanoparticle products are capped by the carboxylic groups of decanoic acid molecules and precipitated in the bottom of the autoclave liner due to their hydrophobic surface in polar water–ethanol environment. This water/ethanol-based approach provides a simple, versatile, high-yield, and inexpensive pathway for the synthesis of erbium-based micro/nano-architectures. The monoclinic ErOOH phase can be obtained at 120–140°C and the cubic Er_2O_3 phase at 160–180°C. Thus, ErOOH and Er_2O_3 particles could be obtained with sizes ranging from 3 nm up to 3 μm and exhibiting various shapes, including spheres, *wrinkle*-surfaced spheres, flowers, wires, rods, bundles, etc. With increasing the concentration of decanoic acid from 0.038 to 0.190 M, the particle size of the product decreased from the micro- to nanometer range. When water/ethanol (10:30 mL) was replaced by anhydrous ethanol, the particle size further decreased from 18 nm (nanospheres) to 3 nm (so-called *nanocores*). Nanorod products were also achieved with high precursor concentrations, e.g., 76.25 to 152.50 mM, due to anisotropic crystal growth.

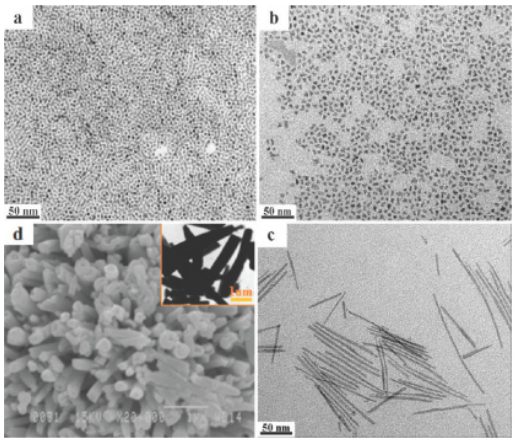

Figure 10.6 TEM/SEM images of the Er_2O_3 samples synthesized with DA/Er 20:1 under different reaction conditions: (a) ~3 nm nanocores, $[Er(NO_3)_3]$ = 7.63 mM without water; (b) ~4 nm nanodots, $[Er(OH)_3]$ = 7.63 mM, ethanol/water = 30:10 (mL); (c) 80 nm × 150 nm nanowires, $[Er(OH)_3]$ = 76.25 mM, ethanol/water = 30:10 (mL); (d) 250 nm × 1000 nm microrods, $[Er(OH)_3]$ = 152.50 mM, ethanol/water = 30:10 (mL) [39].

10.2.2 Two-Phase Routes

The two-phase approach was first developed by Brust *et al.* [40] in 1994 for the synthesis of gold nanocrystals and other noble metal nanocrystals such as Ag, Pt, and Pd. First, a water-soluble gold precursor was transferred into toluene by a phase transfer reagent. Then, an aqueous solution of sodium borohydride was added as a strong reducing agent to induce nucleation and growth. Gold nanocrystals were produced at the toluene/water interface, then capped by hydrophobic ligands, and dispersed in toluene. The surfactant species, consisting of a coordinating head group and a long alkyl chain, adsorb reversibly to the surfaces of the growing nanocrystals and thus provide a dynamic organic capping layer that stabilizes the nanocrystals in solution and also mediates their growth, providing excellent control of the crystallite size and shape. Progress using this two-phase approach was also extended to the synthesis of a variety of nanomaterials under hydrothermal treatment. Compared to the single-phase synthetic route, the two-phase strategy can also provide products with high crystallinity under relatively mild conditions, owing to the presence of the water phase that generally increases the speed of the growth process [41]. Particle size and shape can also be controlled because the nucleation process occurs with relatively slow rate at the interface.

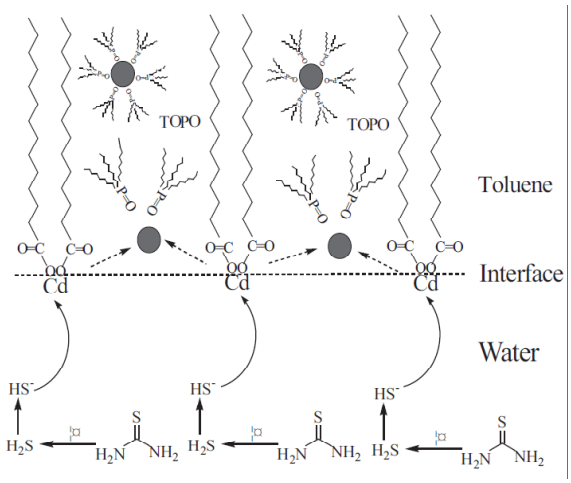

Figure 10.7 The mechanism for forming CdS nanocrystals at a toluene–water interface [42].

Wang *et al.* [42] reported a modified version of the two-phase approach for the synthesis of the CdS nanocrystals, which was produced at the water/toluene interface by mixing a cadmium myristate toluene solution and a thiourea aqueous solution (Fig. 10.7). By this approach, the authors also synthesized the CdSe and CdSe/CdS core/shell nanocrystals using selenourea as the selenium precursor [43]. In all cases, the obtained products had narrow size distribution due to the use of low concentration of reaction precursors.

Pan *et al.* [44] reported on the synthesis of monodisperse TiO_2 nanocrystals from the hydrolysis of titanium(IV) *n*-propoxide in a water–toluene mixture. An alkoxide can be used as titanium precursor; *tert*-butylamine and OA are used as activation agent and capping agent, respectively. Being an indirect bandgap semiconductor, the luminescence of the resulting TiO_2 nanocrystals was studied at room temperature. Ji *et al.* [45] synthesized ZrO_2 nanocrystals with various shapes, including spheres, and rod-like. The shapes of nanocrystals could be tailored by changing the zirconium(IV) *n*-propoxide concentration, the nature of the capping agents, and the reaction temperature. Figure 10.7a,b shows typical TEM images of TiO_2 and ZrO_2 nanocrystals. Kaskel *et al.* [46] also used this method to synthesize $BaTiO_3$ nanocrystals starting from mixed titanium(IV)-*n*-butoxide and barium acetate precursors. Furthermore, Adschiri *et al.* [47] modified this system for the synthesis of CeO_2 nanocubes using cerium hydroxide precursors under supercritical water conditions. The product shape could be varied by tuning the interaction of organic molecules with various crystallographic planes of the fluorite cubic ceria. In contrast to metal alkoxide precursors, metal stearates are cheaper and more stable; Ji *et al.* [48] exploited this advantage and produced Mn_3O_4 nanocrystals using manganese(II) stearate precursors. The spherical and cubic shapes and their particle size were controlled by adjusting the reaction time and concentration of the activation agent, as illustrated on Fig. 10.8c,d.

A modified two-phase method has been reported for the synthesis of alkyl chain-capped metal particles (e.g., Cu and Au) and metal oxide nanoparticles (TiO_2 and ZrO_2), followed by cooperative assemblage of the thus-obtained particles into unusual hybrid metal/metal oxide NCs mesostructured materials [49]. The authors also developed a general two-phase route to synthesize colloidal metal oxide nanocrystals of two-group elements: rare earths, Sm, Ce, Er,

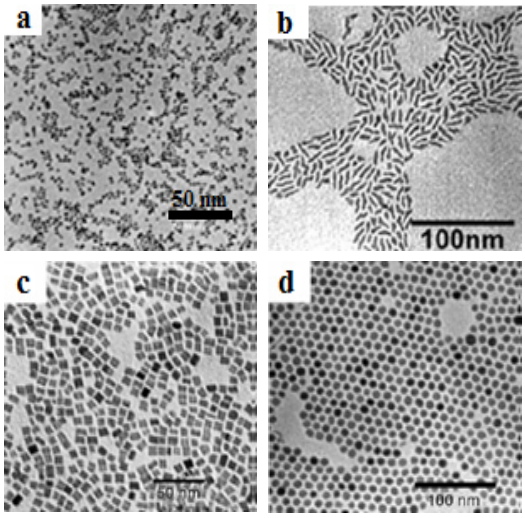

Figure 10.8 TEM images of (a) TiO_2 nanoparticles [44], (b) ZrO_2 nanorices [45], (c) Mn_3O_4 nanocubes, and (d) Mn_3O_4 nanospheres [48].

Gd, La, Y and transition metals, Mn, Cr, Co, Ni [50]. These routes used metal salts under mild reaction conditions, enabling easy control of size and shape, and multigram-scale production. An example is the large-scale synthesis of high-quality metal oxide nanocrystals using inexpensive metal nitrate salts in the presence of a fatty acid as a capping surfactant agent. In this way, the metal hydroxides formed under basic solution due to hydrolysis of *tert*-butylamine in water generated OH^- ions. The nanocrystalline oxide was obtained by dehydration of the metal hydroxides at the water–toluene interface upon hydrothermal treatment (180°C for 24 h).

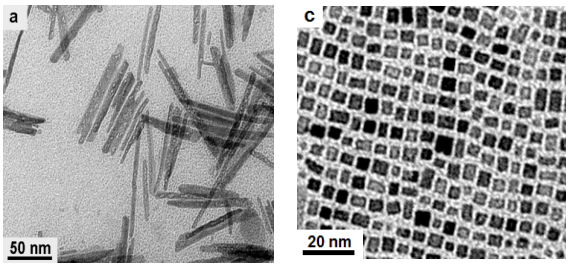

Figure 10.9 TEM images of the (left) Sm_2O_3 nanorods and (right) CeO_2 nanocubes/elongated nanocubes synthesized using the corresponding metal nitrate salts [39].

10.2.3 Thermal Decomposition

Nanocrystals with controlled size and shape can be synthesized through the thermal decomposition of organometallic compounds in high-boiling organic solvents containing stabilizing surfactants, as schematically shown in Fig. 10.10 [51–54]. In general, this procedure involves the injection of a room temperature solution of the molecules into a hot organic solvent in the presence of surfactants. Nonhydrolytic thermal decomposition procedures that produce uniform nanocrystals are widely implemented, and typical organometallic complex precursors include metal acetylacetonates, metal acetates, metal oxalates, metal cupferronates, metal alkoxides, metal carbonyls, etc. Fatty acids, aliphatic amines, alkyl phosphonic acids, and alkyl thiols are often used as surfactants. Here again, the ratios of the starting reagents, including organometallic compound, surfactant, and solvent, as well as reaction temperature and time are the decisive parameters for the precise control of the size and shape of the nanocrystals. The identification of suitable molecular precursors, the regulation of solvent-coordinating capability, and the balance of the nucleation and growth stages are the three key elements for obtaining high-quality products. In contrast to the two-phase method, this seed-mediated growth method is the separation of nucleation and growth, because it involves the addition of preformed nuclei to a reaction solution containing the monomers that subsequently adsorb on the surface of these very small particles without new particle nucleation.

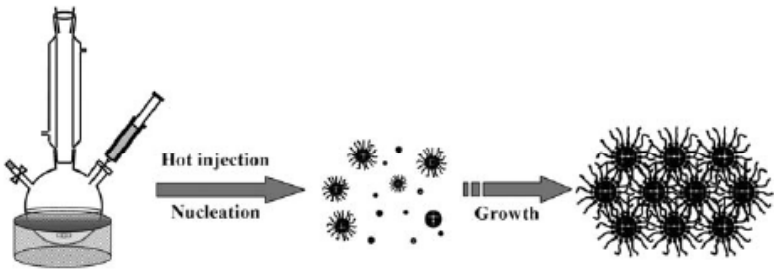

Figure 10.10 Thermal decomposition procedure for the synthesis of monodisperse nanocrystals [54].

As early as 1993, Murray and colleagues [55] developed the hot injection approach for the controllable synthesis of suspensions of

almost monodisperse CdE (E = S, Se, Te) nanocrystals in organic solvents, showing a bright luminescence and a clearly resolved, discrete optical transitions. This synthetic strategy became one of the most popular liquid-phase routes toward inorganic nanomaterials. The Hyeon group [56] reported the reaction of zero-valent metal carbonyl precursors with a chemical oxidant to yield monodisperse FeO nanocrystals in the size range of 4–16 nm. The particles are obtained by decomposing $Fe(CO)_5$ complexes in octyl ether at 300°C in the presence of OA. Subsequently, addition of trimethylamine oxide $(CH_3)_3NO$ as a mild oxidant at elevated temperature under aging conditions results in the formation of monodisperse 13 nm-sized Fe_2O_3 nanocrystals. MnO nanorods were also obtained from air oxidation of $[Mn(CO)_{10}]$ complexes in a similar reaction system [57]. The authors also revealed that monodisperse iron nanoparticles with different sizes (4, 8, and 11 nm) were prepared by changing the $Fe(CO)_5$:OA molar ratio from 1:1 to 1:2 and 1:3. In the next step, these nanocrystal seeds are reacted with iron oleate solutions of given concentrations, resulting in monodisperse iron nanocrystals that are converted into iron oxide nanoparticles of 6, 7, 8, 9, 10, 11, 12, and 13 nm on exposure to air (Fig. 10.11) [58]. The small size distribution leads to the self-assembly of the iron oxide nanocrystals in a hexagonally ordered structure on the TEM grid. Park *et al.* [59] showed that the WO_{3-x} nanorods may be prepared by the similar injection of $[W(CO)_6]$ into a solution of octyl ether and OM at boiling solvent temperature. Similar results for the preparation and size control of polycrystalline Mo/MoO_x nanoflakes were also reported by Song *et al.* [60]. The subsequent transformation to single-crystalline MoO_3 and MoS_2 nanocrystals with an average diameter of 2 nm is shown possible by *in situ* addition of oxygen and sulfur into the colloidal solution. This route was also applied for the synthesis of manganese ferrite nanocrystals. Similarly, iron–manganese alloy nanocrystals were first formed by the thermal decomposition of Fe–Mn–oleate complexes, the resulting alloy nanocrystals being then oxidized using Me_3NO to obtain manganese ferrite nanocrystals [61].

The Niederberger group [62] using only $M(acac)_x$ precursors and benzylamine solvent produced a family of transition metal oxide nanocrystals. Following this, a number of nanocrystals of Co_3O_4, Cr_3O_4, Fe_2O_3 with specific shapes were prepared from

the corresponding Metal(acac)$_x$ precursors by O'Brien *et al.* [56] and Peng *et al.* [63]. Hyeon group [64] recently also reported the synthesis of uniform magnetite Fe_3O_4 nanocubes ranging from 20 to 160 nm in size using a reaction medium of iron(III) acetylacetonate, OA, and benzyl ether. The ferrimagnetic nature of the Fe_3O_4 nanocubes was characterized and application for magnetic separation of histidine-tagged protein was studied. Cube-shaped $CoFe_2O_4$ nanocrystals were obtained through thermal reactions of cobalt(II) acetylacetonate and iron(III) acetylacetonate in the presence of OA and OM [65]. Under mild crystal growth conditions with a low precursor concentration and a slow heating rate, cube-shaped $CoFe_2O_4$ nanocrystals were obtained (Figure 12), whereas spherical-shaped nanocrystals were formed under harsher growth conditions (e.g., high temperature and high precursor concentration). The use of acetate precursors in the preparation of metal oxide nanocrystals appears safer, less expensive, and more environmentally benign than their metal carbonyl counterparts. The nanocrystal products are of comparable uniformity and monodispersity. The acetate precursors also possess low moisture sensitivity, rendering them less prone to hydrolysis, which is a common disadvantage for metal alkoxides and halides. Cao *et al.* synthesized the Gd_2O_3 nanoplates through the thermolysis of $Gd(O_2CCH_3)_3$ in a hot octadecene containing OA and OM surfactants under argon atmosphere. These nanoplates assemble into ribbons of stacked plates that stand on their edges [66].

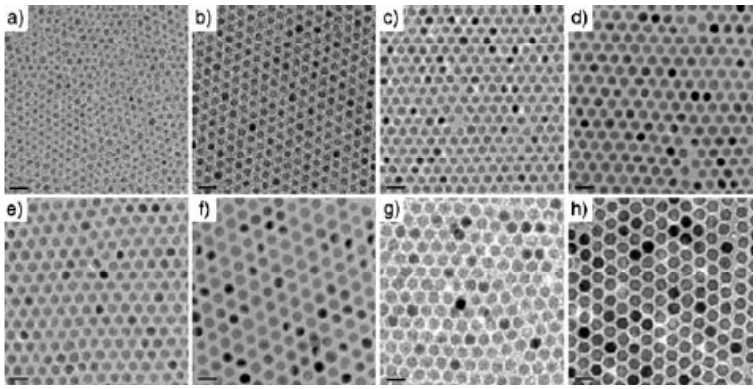

Figure 10.11 TEM images of monodisperse iron oxide nanospheres with particle sizes of (a) 6, (b) 7, (c) 8, (d) 9, (e) 10, (f) 11, (g) 12, and (h) 13 nm. Scale bar is 20 nm [58].

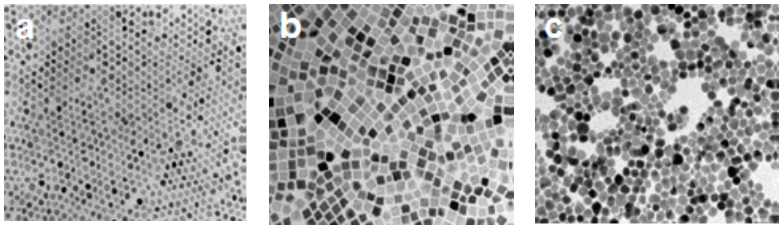

Figure 10.12 TEM images with the scale bar as 50 nm of highly crystalline iron ferrite nanocrystals: (a) 7.9 ± 0.5 nm spherical $CoFe_2O_4$ nanocrystals, (b) 9.1 ± 0.5 nm cubic $CoFe_2O_4$ nanocrystals, and (c) 11.8 ± 1.3 nm spherical $CoFe_2O_4$ nanocrystals [65].

Recently, the Hyeon group [67] yielded single unit-cell-thick Sm_2O_3 nanowires/nanoplates as well as high-quality Mn_3O_4 nanocrystals [68] with various shapes from the thermal decomposition of the corresponding metal(III) acetates. The 9 nm-sized Mn_3O_4 nanoplates dispersed in organic solvent were coated with a poly(ethylene glycol) (PEG)-phospholipid shell to make them water-dispersible and biocompatible. This property was used as contrast agent for magnetic resonance imaging. Furthermore, the cobalt stearate precursor ($Co(O_2CC_{17}H_{35})_2$) decomposes thermally in a hot organic solvent containing stearic acid to form triangular Co_3O_4 nanocrystals [69]. Similarly, triangular crystals of NiO and rod-like ZnO nanostructures were obtained from metallic myristate precursors. Martyn *et al.* [70] also used this strategy to prepare a number of spinel ferrite NC samples, starting from mixtures of different Fe(II) and M(II) acetates (M = Co, Ni, Zn). The extension of such methods to reach a generalized synthesis of 2D lanthanide oxide nanoplates was proven possible [71].

Thermal decomposition of a transition metal alkoxide precursor in a hot organic solvent can also induce 1D growth of metal oxide nanocrystals. Weller *et al.* [72] reported the synthesis of TiO_2 nanorods through thermal decomposition of a $Ti(OiPr)_4$ precursor in the presence of OA. The authors observed that the presence of surface-selective surfactants may hinder an oriented attachment during hydrothermal growth. The formation of the observed shapes was the anisotropic growth through the addition of monomers onto the high energy surface**.** Cheon *et al.* [73] reported a generalized approach for synthesis of transition-metal oxide nanorods, including $W_{18}O_{49}$, Mn_3O_4, and TiO_2, through a thermal reaction of metal halides

and OM. The reaction of metal halides and OA induces an increase of the metal oxide monomer concentration and promotes fast growth of nanocrystals along directions having high surface energy. A major drawback of the traditional hot-injection method is the use of expensive, hazardous, and toxic organometallic precursors, and this has motivated many groups to develop alternative methods based on cheaper and less hazardous chemicals. The Hyeon group [74] used nontoxic and inexpensive iron(III) chloride and sodium oleate to generate an iron oleate complex *in situ*, which was then decomposed at temperatures between 240 and 320°C in different solvents, such as 1-hexadecene, octyl ether, 1-octadecene, 1-eicosene, or trioctylamine. Particle sizes were in the range of 5–22 nm, depending on the decomposition temperature and aging period, i.e., aging was found to be a necessary step for the formation of iron oxide nanocrystals. Subsequently, the resulting nanocrystals were used as particle precursors to prepare the corresponding uniform hollow oxide nanocrystals through a nanoscale acid etching [75].

10.2.4 Microemulsions

A microemulsion is a transparent and thermodynamically stable solution of low viscosity that forms spontaneously from the mixture of surfactant, water, and oil. A water-in-oil (W/O) microemulsion is a solution of water droplets of nanometer size dispersed in a hydrocarbon phase with the aid of a monolayer of surfactant molecules [76–78]. The size of the reverse micelles is determined by the molar ratio of water to surfactant. A microemulsion can be used as a nanoreactor for the production of nanoparticles of uniform size through chemical reactions confined within the aqueous core. The thus-formed nanoparticles are stabilized by the surfactant layer acting as steric stabilizers to inhibit the aggregation of nanoparticles formed [79]. By the addition of solvent, such as acetone or ethanol, the precipitate can be extracted by filtration or centrifuging the mixture.

The droplet size can increase to a dimension (~2–20 nm) that is much larger than the monolayer thickness of the surfactant because the inside reservoir of water or oil may be enlarged. By changing the water pool size, the particle size can be controlled. As the surfactant concentration increases further, micelles can change into different shapes. Microemulsions are considered to be almost monodispersed

and are in a dynamic state that involves constant collisions between droplets. Depending on the interaction potential between the droplets, which is determined by the fluid (e.g., oil), the surfactant used, and some collisions, the result is coalescence. Once the droplets coalesce, the coalesced droplets tend to break up because these are not as thermodynamically stable as the original droplets. Thus, unless the interactions between droplets are very repulsive, the aqueous droplets in a water-in-oil microemulsion undergo continuous coalescence and break up, which results in continuous exchange of the droplet contents. When two microemulsions are mixed, each of them containing the respective reactants, the contents of the aqueous droplets are mixed and redistributed (Fig. 10.13). This process is very rapid because of collisions that involve temporary merging of the droplets into larger droplets and subsequent breakup of these larger droplets. This ultimately leads to the formation of a precipitate inside the micelles. It was found that the mass exchange between the droplets can be extremely fast and consequently, it is only limited by the collision rate of the droplets. The particles prepared in such microemulsion solutions are generally very fine and monodisperse [15, 79].

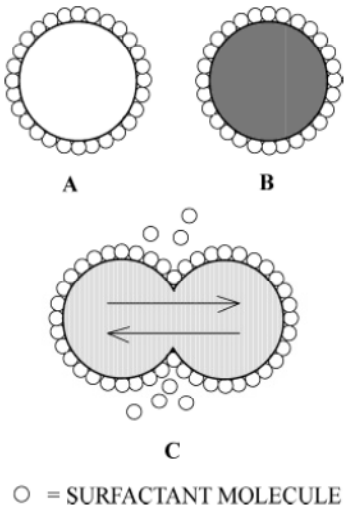

Figure 10.13 Schematic of a collision between two reverse micelles with dissimilar cores. The micelles form a short lived dimer, as some surfactant molecules are released into the oil phase and the contents of the micellar cores are exchanged [15].

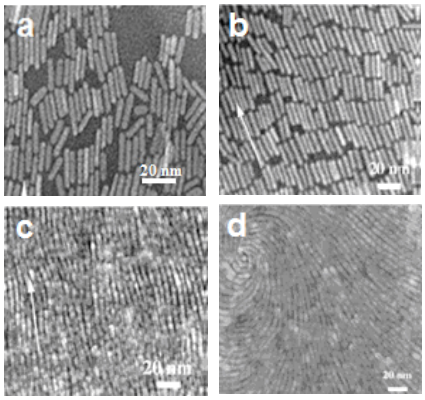

Figure 10.14 TEM images of $BaCr_2O_4$ nanocrystals: (a) isotropic phase, (b) 3D nematic phase, (c) 2D smectic phase, and (d) 3D nematic phase [84].

Using the microemulsion technique, a variety of nanocrystals has been successfully synthesized in the recent years. Seal *et al.* [80] synthesized 40 nm × 250 nm-sized CeO_2 nanorods by self-assembly of nanoparticles in a water/AOT/toluene microemulsion. Initially, a hydrogen peroxide solution was added to the water/AOT/toluene microemulsion containing Ce^{3+}. Mutual interactions among two such types of micelles took place by random collisions. Transfer of reactants occurred to form the nanoparticles in the inner core of each reverse micelles. The presence of coordinated surfactant molecules around the spherical nanoreactor prevented pronounced aggregation of the ceria nanoparticles. Self-assembly of ceria nanoparticles then led to gradual evolution into ceria nanorods upon aging. The presence of nitrate ions from the precursor solution in the present situation may also have influenced the interfacial properties of the micelles in such a way that the process of the formation of supra-aggregates was facilitated. A general emulsion-based bottom-up self-assembly approach was developed to assemble various kinds of nanocrystal building blocks with different compositions, shapes, and sizes into 8 nm-sized $BaCrO_4$ nanospheres [81]. The composition, size, and surface charge of the $BaCrO_4$ nanospheres could be controlled. Mann *et al.* [82, 83] demonstrated this principle by producing three different $BaCrO_4$ nanostructures — linear chains, rectangular superlattices and long filaments — as a function of reactant molar ratio, which in turn is controlled by fusing reverse micelles and microemulsion droplets containing fixed concentrations of barium and chromate

ions, respectively. Interestingly, Yang *et al.* [84] reported the formation of liquid-crystalline phases of $BaCr_2O_4$ nanorods through Langmuir–Blodgett assembly process. By increasing the surface pressure, various liquid-crystalline phases could be obtained ranging from isotropic to 2D nematic, 2D smectic, 3D nematic, and spiral phases (Fig. 10.14).

10.3 Shape Control of Metal Oxide Colloidal Nanocrystals

In colloidal solutions, evolution of nanocrystal growth is driven by the interplay between thermodynamic factors (e.g., relative stability of crystal polymorphs) and kinetically limited processes (e.g., diffusion of reactants, surface adhesion of surfactants). However, control over most of these parameters can be achieved by judicious adjustment of just a few experimental conditions, such as the type and the relative concentration of molecular precursors, catalysts, and organic stabilizers, in combination with a suitable growth temperature [85]. Metal oxide nanocrystals in a variety of shapes such as spheres, cubes, rods, wire, disks, and polypods have been achieved by controlling these parameters. In this section, we will discuss some major strategies for the shape control of metal oxide nanocrystals.

10.3.1 Shape Control by Oriented Attachment

The classical crystal growth kinetics Ostwald ripening theory is commonly used to explain the diffusion-controlled crystal growth process. In this process, the formation of tiny crystalline nuclei in a supersaturated medium occurs first and then it is followed by crystal growth, in which the larger particles will grow at the expense of the small ones due to the energy difference between large particles and the smaller particles of a higher solubility based on the Gibbs–Thompson law. In nanoscale systems, another significantly important mechanism is designated as ‘‘oriented attachment,’’ where nanoparticles with sharing crystallographic orientations directly combine together to form larger ones [86]. The concept of “oriented attachment” was first demonstrated by Banfield and his team who studied the hydrolytic synthesis of TiO_2 nanocrystals [87]. Truncated diamond-shaped anatase TiO_2 nanocrystals have three

different faces: {0 0 1}, {1 2 1}, and {1 0 1}. Since the (0 0 1) face has the largest number of dangling bonds and the (1 0 1) face has the lowest number of dangling bonds, the surface energy of the (0 0 1) face is higher than that of the (1 0 1) face. When there is a sufficient thermal energy in the system, the suppression of the high-energy surfaces is thermodynamically favorable. Therefore, the fusion between diamond-shaped nanocrystals along the [0 0 1] direction is facilitated by oriented attachment process, resulting in necklace-shaped nanostructure crystal (Fig. 10.15).

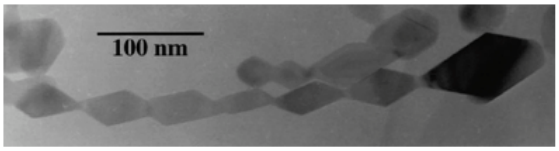

Figure 10.15 A neckless-like single crystal of anatase that was hydrothermally coarsened in 0.001 M HCl and grown by the oriented attachment mechanism [87].

Oriented attachment was also found to be an effective route for the transformation of small nanocrystals to larger ones [86]. Weller *et al.* [88] demonstrated that perfect ZnO nanorods can be self-assembled from small ZnO quasi-spherical nanoparticles. Reflux treatment of a concentrated solution of a ZnO sol with average particle size of about 3 nm leads to the formation of rod-like nanoparticles. Prolonging the heating time induces an elongation of the particle along the c-axis. After refluxing for one day, single crystalline nanorods with average lengths of 100 nm and widths of approximately 15 nm were observed (Fig. 10.16).

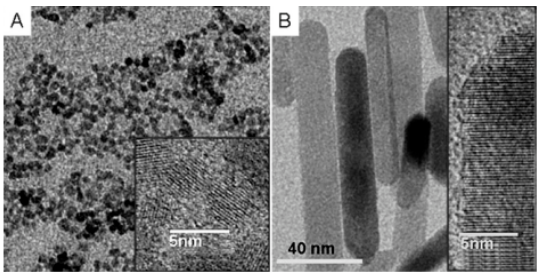

Figure 10.16 TEM images of ZnO. (A) starting sol; (B) after one day reflux of the concentrated sol. The insets show high-resolution TEM images of individual nanoparticles [88].

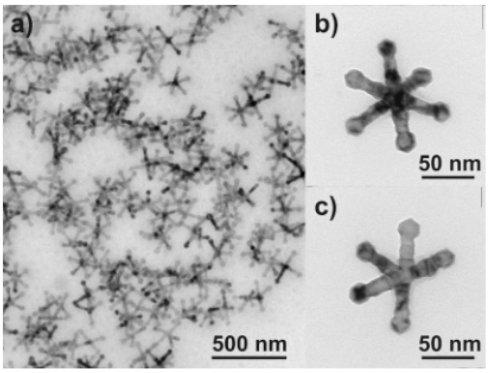

Figure 10.17 Overview TEM image of an assembly of MnO multipods (a), a hexapod (b), and a pentapod (c) [89].

Another interesting example of oriented attachment is observed in the synthesis of MnO multipods [89] (Fig. 10.17). The MnO multipods were synthesized based on the thermal decomposition of $Mn(oleate)_2$ in n-trioctylamine. TEM micrographs show that most of the multipods appeared to be hexapods (Fig. 10.17b), however 2, 3, 4, or 5 pods (Fig. 10.17c) were also found in the sample. The cores and pods were found to be uniform in size and morphology, each arm being terminated by an "arrow." Considering the cubic rock salt structure of MnO, anisotropic crystal growth is unexpected. To explain this behavior, a two-step mechanism has been proposed, involving nucleation of truncated octahedra or cubes, followed by oriented attachment of these nanoparticles into the final pod morphology.

The oriented attachment mechanism was also applied in the synthesis of rare earth metal oxide and mixed oxides [90]. Nguyen *et al.* reported the formation of Sm_2O_3 nanorods from Sm_2O_3 nanoparticles using a two-phase hydrothermal route. At a relatively low synthesis temperature (120°C), monodisperse platelet-like nanoparticles were obtained as the sole products with a diameter of about 5 nm. When the reaction temperature was increased to 140°C, after 24 h, a mixture of spherical particles and rod-like particles were observed. This can be explained by Ostwald ripening. This means that the size control of nanorods (length and width) through oriented aggregation can be achieved by controlling primary particle size and reaction temperature.

10.3.2 Shape Control by Surface Energy and Selective Adhesion

The shape of a crystal is determined by the relative specific surface energies associated with the facets of the crystal. At equilibrium, a crystal has to be terminated by facets giving a minimum total surface energy [91]. Since the crystal growth rate is correlated exponentially to the surface energy, surface-energy differences induce much faster growth of the higher surface energy planes and keep the slower growing planes (lower surface energy) as the facets of the product. The surface energy of the nanocrystals can be modulated by introducing surfactants that adsorb onto surfaces of the growing crystallites [92].

Selective adhesion of surfactants has been widely used for the shape-controlled synthesis of a variety of metal oxides [31, 37, 66, 71, 93]. Anatase TiO_2 nanocrystals are perfect model system for surface-energy modulated anisotropic growth [93]. When TiO_2 with a truncated octahedral, bipyramidal shape terminated by {001} and {101} faces nucleates, fast growth along the high-energy surface {001} leads to the formation of arrow- and diamond-shaped nanocrystals. However, when lauric acid was used as surfactants, they strongly bind to {001} faces and reduce the growth rate along the <001> directions and, consequently, results in the formation of nanorods. TiO_2 anatase nanocrystals with a variety of shapes could also be obtained using two kinds of surfactants that selectively adsorb on different faces of the anatase crystals. Thang *et al.* [31] reported the shape evolution of TiO_2 nanocrystals by adjusting the OA:OM molar ratio in the synthesis mixture. It is found that, when the OA/OM ratio is less than 4:6, only rhombic-shaped TiO_2 nanocrystals are formed. When this ratio is higher than 6:4, the nanocrystal size decreases markedly and nanodots of TiO_2 are obtained. In the absence of OA, only the rhombic shape was observed, whereas a mixture of spherical particles and nanodots is produced in the absence of OM. These results confirmed a cooperative effect of the combination of OA and OM on the resulting particle shapes. The shape of TiO_2 NCs is determined by the growth rate ratio between [001] and [101] directions. In the absence of OA or at low OA/OM ratio, hydrolytic reactions are predominant in this system, and the formation of nanoparticles is thus a fast process. Due to high surface energy of the {001} faces, growth along [001] is occurring progressively, leading to

the depletion of the {001} faces. In contrast, the low surface energy of {101} faces and the adhesion of OM to these faces hinder the growth along the [101] direction. As a result, rhombic-shaped TiO_2 nanocrystals are obtained. Increasing the OA/OM ratio slows down the rate of the reaction. The presence of a relatively large amount of OA limits the growth along [001] as OA binds selectively to the {001} faces. Consequently, the surface area of the {001} surfaces is preserved. Crystals grow on both {001} and {101} faces, leading to the truncated rhombic or spherical nanocrystals. However, when a large excess of OA is used (OA/OM ratio > 6:4), the growth process undergoes nonhydrolytic condensation rather than a hydrolytic one. Since OA can be adsorbed on almost the entire surface of TiO_2, the crystals grow mainly on the high surface energy faces (i.e., {001} faces), leading to the formation of nanodots and nanorods.

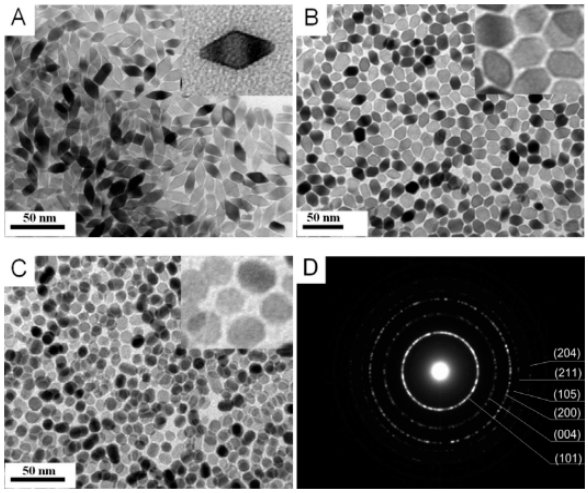

Figure 10.18 TEM images of (A) the rhombic shapes obtained at TB/OA/OM 1:4:6; (B) truncated rhombic shape obtained at TB/OA/OM 1:5:5; (C) spherical shape obtained at TB/OA/OM 1:6:4. Insets show high-magnification images of the corresponding shapes. (D) SAED of truncated rhombic TiO_2 nanoparticles [31].

Selective adsorption was also applied for the shape control of mixed metal oxide nanocrystals. For example, the shape and size of $SmVO_4$ nanocrystals were controlled by the nature and amount of capping surfactant as well as concentration of the chosen metal

complex precursor using a solvothermal method [37]. The use of surfactants with selectivity toward specific crystal faces, or mixtures of surfactants with different binding affinities for the nanocrystal surface, allows excellent shape control. Figure 10.19 displays TEM images of the $SmVO_4$ nanospheres and nanohexagons obtained using two different OM and OA surfactants.

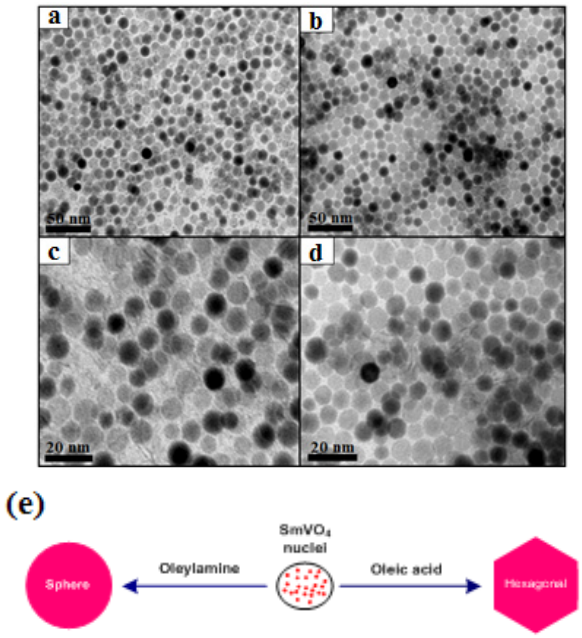

Figure 10.19 TEM images at different magnifications of the $SmVO_4$ nanocrystals prepared using two different surfactants: (a,b) using oleylamine, nanospheres, (c,d) using oleic acid, nanohexagons, and (e) schematic representation of the effect of capping surfactant on the shape of the nanocrystals products [37].

10.3.3 Shape Control by Control of the Growth Regime

A balance between the kinetic and the thermodynamic growth regimes governs the final shape of the nanocrystals. Isotropic growth of nanocrystals is preferred under the thermodynamic growth regime that is characterized by a sufficient supply of thermal energy and a low flux of monomers. In contrast, anisotropic growth along a

specific direction is facilitated under a kinetic growth regime that is promoted by a high flux of monomers [13].

Several kinds of nanocrystals with controlled size and shape have been synthesized by controlling the growth regime [31, 50, 94, 95]. An example is the shape evolution of TiO_2 nanocrystals under solvothermal treatment at different temperatures [31]. When the temperature was 120°C, small TiO_2 nanorods were obtained. Increasing the temperature to 140°C led to the formation of uniform nanobars of TiO_2 with a size of ca. 11 × 20 nm. When the reaction was performed at 160°C, a mixture of spherical particles and nanorods of TiO_2 was observed. Further increase in the temperature to 180°C yielded uniform TiO_2 nanocrystals with spherical shape (Fig. 10.20). Thus, when the reaction temperature is increased, the shape of TiO_2 nanocrystals evolved from an anisotropic form to an isotropic one (i.e., from nanorods to spherical particles). This can be ascribed to the balance between the kinetic and thermodynamic growth regimes. In the kinetic regime, the crystals grow rapidly on the faces with high surface energy, leading to TiO_2 nanorods. However, when the growth temperature is increased to a value that provides sufficient thermal energy, the shape of TiO_2 nanocrystals changes to more thermodynamically stable sphere-like through intraparticle ripening and interparticle Ostwald ripening processes.

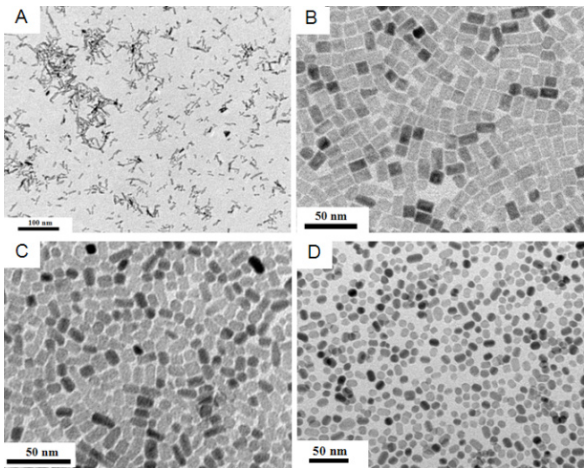

Figure 10.20 TEM images of TiO_2 nanocrystals obtained with TB:OA:OM = 1:6:4 at different reaction temperatures: (A) 120; (B) 140; (C) 160; and (D) 180°C [31].

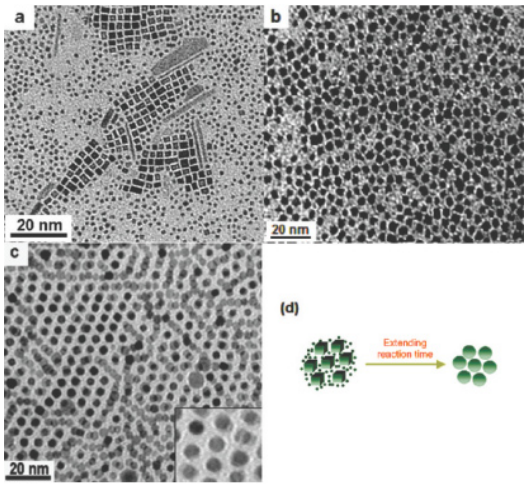

Figure 10.21 TEM images of Co_3O_4 obtained at different times: (a) 12 h, a mixture of nanocubic and nanocubic self-assemblies (sample 12), (b) 18 h, nanocubes (sample 11), (c) 24 h, self-assemblied nanospheres nanospheres (sample 10) [50].

Another example for the growth regime effect is the shape evolution of Co_3O_4 nanocrystals under solvothermal condition with different treatment times [50]. In the early stages, Co_3O_4 nanocubes could be formed following anisotropic growth. Nanocubes with six crystal faces of {100}, {010}, and {001} were formed by the specific growth of the {111} facets of the cuboctahedral clusters. When extending the reaction time, the monomer Co(II)-oleate complex concentration gradually depleted via the nucleation and growth of the nanocrystals. If the reaction time is sufficiently long (in this case, 24 h), the monomer concentration should drop to a level that is a lower than that required for a given cubic shape. The cubic shape should eventually evolve into a spherical shape, which is the most stable shape, by displacing monomers from the {111} to the {100} faces because of the differences of chemical potential between these two faces.

10.3.4 Shape Control Using Dopants

Doping is a widely applied technological process that involves incorporating atoms or ions of appropriate elements into host lattices to generate desirable properties and functions. Recent

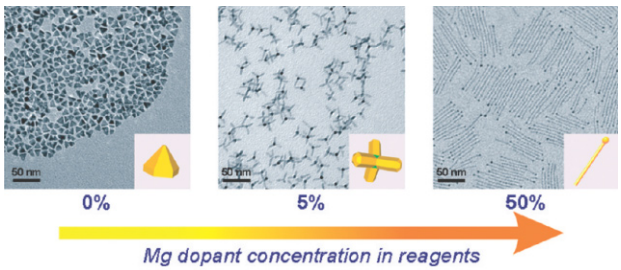

Figure 10.22 Representative TEM images of the nanocrystals from the 0%, 5%, and 50% $Mg(St)_2$ reactions, emphasizing the shape evolution of colloidal nanocrystals due to the increasing concentration of Mg dopant in the synthesis mixture (highlighted by the arrow). Insets are the corresponding three-dimensional models of the nanocrystals (not to scale) [100].

studies demonstrated that the presence of dopants also affects the stabilizing of a specific crystallographic phase and, consequently, the growth of the crystals [96–100]. In 2006, Wang and co-workers [96] reported the conversion of CeO_2 nanopolyhedra into nanospheres by Ti^{4+} doping. Ceria system was doped with titanium, using flame temperatures that facilitate crystallization of the ceria and yet retain the titania in a molten state. Under these conditions, the inner ceria core evolves in a single-crystal spherical shape without faceting, because throughout the crystallization it is completely encapsulated by a molten 1- to 2-nanometer shell of titania that, in liquid state, minimizes the surface energy. Dopant-induced shape evolution was also applied to control the shape and structure of In_2O_3 nanocrystals [97]. The presence of Cr^{3+} and Mn^{3+} dopants adsorbed on the surface of colloidal In_2O_3 nanocrystals during incorporation inhibits nanocrystals growth. This phenomenon induces a surface stress that gives rise to a reduction in atomic volume and leads to the formation of metastable corundum-type In_2O_3 for nanocrystals smaller than 5 nm. The growth beyond the critical reduces the potential energy barrier height and causes a nanocrystal phase transformation. Very recently, Yang *et al.* [100] reported that in the synthesis of ZnO nanocrystals, introduction of Mg dopants leads to dramatic shape evolution, in addition to the expected compositional variation of the resulting nanocrystals. Depending on the relative concentrations of the dopant precursor, Mg-doped ZnO nanocrystals with well-defined shapes, from tetrapods to ultrathin nanowires, were obtained, which exhibit tunable optoelectronic

properties (Fig. 10.22). Mechanistic studies have shown that at the primary growth stage, the incorporation of Mg^{2+} ions into the ZnO seeds significantly influences the growth of the host lattices. The relative concentration of dopant precursor in the synthesis medium is one of the key factors that drives initial growth of seeds with different crystallographic phases and shapes and eventually leads to doped nanocrystals with different morphologies.

10.3.5 Shape Control by a Confinement in an Inorganic Network

The shape control of metal oxide nanoparticles can also be achieved by confining the growth of the particles in an inorganic network. In principle, the metal oxide nanoparticles are grown inside the void of an inorganic material (denoted as a hard template); consequently, the size and the shape of the void in the template will determine the morphology of the resulting metal oxide nanoparticles. In addition, the morphology of the metal oxides can also be controlled by varying the amount of metal precursors loaded into the void. Several inorganic, ordered porous solids such as zeolites, alumina membranes, ordered mesoporous silica, or ordered mesoporous carbon have been used as a nanoscale template for the synthesis of nanostructured metal oxide materials [101]. Among them, ordered mesoporous silica is the most versatile hard template not only because of the high surface area and high pore volume but also because it can be prepared in a variety of shapes such as noodle-like, spherical, fibrous, or rod-like with different pore structure, including two- and three-dimensional ones [102]. The pathway for the synthesis of nanostructured metal oxide using ordered mesoporous silica as hard template, denoted as nanocasting, is illustrated in Fig. 10.23.

Figure 10.23 Schematic illustration of the nanocasting pathway, showing the change of the mesostructure during the process. In general, the process includes three steps: (i) precursor infiltration inside the mesochannels of the silica template; (ii) conversion of the precursor inside the nanochannels; (iii) selective removal of the mesoporous silica template [102].

One example for the shape control of metal oxide nanoparticles by nanocasting technique is the synthesis of Co_3O_4 using hexagonally ordered mesoporous SBA-15 silica as hard template [103, 104]. The morphologies of the Co_3O_4 nanostructure can be tuned from isolated or randomly organized nanowires to fully interconnected ordered networks of nanowires, by a careful selection of the degree of network interconnectivity of the parent silica and the metal oxide precursor loading.

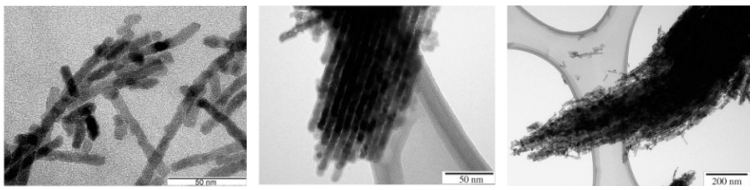

Figure 10.24 TEM images of nanocasted Co_3O_4 with different cobalt precursor loading: from left to right, 15%, 18%, and 24% [103].

10.4 Summary

Nanoscale metal oxides play an important role in the different fields of nanoscience and nanotechnology, e.g., biology, chemistry, physics, materials science, from electronics to nanomedicine. The preparation of metal oxide nanocrystals can be achieved through many different approaches by either physical or chemical methods. Among them, the surfactant-assisted pathways are the most easily controlled for the size, shape, composition, and phase structure of the resulting nanocrystals. The importance of the surfactant is highlighted by the fact that nanocrystals produced by colloidal routes are generally considered together with the surfactants that coat them. This organic coating allows for additional synthetic flexibility in that the surfactants can be substituted to different organic molecules with different functional groups or polarity.

Although there have been many new interesting developments in the shape control of metal oxide nanocrystals in the past few years, there is still a great deal of work to be done. Current shape control strategies still rely highly on experimental trial-and-error approaches rather than on rational design of synthetic strategies. The next step should focus on the development of more versatile

and reliable but simple synthetic schemes for tailored architecture of nanocrystals with desired components. Concurrently, a better understanding of the guiding principles of crystal growth at the nanoscale level should be pursued. This knowledge will enable further fine tuning of the size, shape, and surfaces, and thus functionalities, of nanocrystals. Additionally, the synthesis of hybrid nanocrystals in which nanocrystals of different shapes and properties are connected together in a single particle is also a fascinating subject. The success in synthesizing such multi-component nanocrystals will open access to a completely novel generation of colloidal structures with prospects of optoelectronic, magnetic, biomedical, photovoltaic, and catalytic applications with high level of performance.

References

1. Liz-Marzán, L. M., and Kamat, P. V. (2004). *Nanoscale Materials* (Kluwer Academic Publishers).
2. Kinge, S., Calama, M. C., and Reinhoudt, D. N. (2008). Self-assembling nanoparticles at surfaces and interfaces, *Chem. Phys. Chem.*, **9**, pp. 20–42.
3. Na, H. B., Song, I. C., and Hyeon, T. (2009). Inorganic nanoparticles for MRI contrast agents, *Adv. Mater.*, **21**, pp. 2133–2148.
4. Klabunde, K. J. (2001). *Nanoscale Materials in Chemistry* (John Wiley & Son, Inc.).
5. Schmid, G. (2004). *Nanoparticles: From Theory to Application* (Wiley-VCH Verlag GmbH & Co. KgaA, Weinheim)
6. Niederberger, M., and Pinna, N. (2009). *Metal Oxide Nanoparticles in Organic Solvents* (Springer).
7. Rodríguez, J. A., and Fernández-García, M. (2007) *Synthesis, Properties, and Applications of Oxide Nanomaterials* (John Wiley & Sons, Inc.).
8. Caseri, W. (2004). In Encyclopedia of Nanoscience and Nanotechnology (Nalwa, H. S., Ed.), American Scientific Publishers: Stevenson Ranch, CA.
9. Rao, C. N. R., Muller, A., and Cheetham, A. K. (2007). *Nanomaterials Chemistry* (Wiley-VCH:Weinheim, Germany).
10. Li, L.-S., Hu, J., Yang, W., and Alivisatos, A. P. (2001). Band gap variation of size- and shape-controlled colloidal CdSe quantum rods, *Nano Lett.*, **1**, pp. 349–351.

11. Hu, J., Li, L.-S., Yang, W., Manna, L., Wang, L.-W., and Alivisatos, A. P. (2001). Linearly polarized emission from colloidal semiconductor quantum rods, *Science*, **292**, pp. 2060–2063.
12. Cao, G. (2004). *Nanostructures & Nanomaterials* (Imperial College Press).
13. Sperling, R. A., and Parak, W. J. (2010). Surface modification, functionalization and bioconjugation of colloidal inorganic nanoparticles, *Phil. Trans. R. Soc. A*, **368**, pp. 1333–1383.
14. Jun, Y. W., Choi, J. S., and Cheon, J. (2006). Shape control of semiconductor and metal oxide nanocrystals through nonhydrolytic colloidal routes, *Angew. Chem. Int. Ed.*, **45**, pp. 3414–3439.
15. Cushing, B. L., Kolesnichenko, V. L., and O'Connor, C. J. (2004). Recent advances in the liquid-phase synthesis of inorganic nanoparticles, *Chem. Rev.*, **104**, pp. 3893–3946.
16. Li, Y. D., Liao, H. W., Ding, Y., Fan, Y., Zhang, Y., and Qian, Y. T. (1999). Solvothermal elemental direct reaction to CdE (E = S, Se, Te) semiconductor nanorod, *Inorg. Chem.*, **38**, pp.1382–1387.
17. Deng, Z. X., Wang, C., Sun, X. M., and Li, Y. D. (2002). Structure-directing coordination template effect of ethylenediamine in formations of ZnS and ZnSe nanocrystallites via solvothermal route, *Inorg. Chem.*, **41**, pp. 869–873.
18. Deng, Z. X., Li, L. B., and Li, Y. D. (2003). Structure and magnetic properties of tetraarylporphinatomagnesium(II) electron transfer salts of 2,3,5,6-tetrafluoro-7,7,8,8-tetracyanoquinodimethane, $TCNQF_4$, *Inorg. Chem.*, **42**, pp. 2311–2322.
19. Xu, J., Ge, J. P., and Li, Y. D. (2006). Solvothermal synthesis of monodisperse PbSe nanocrystals, *J. Phys. Chem. B*, **110**, pp. 2497–2501.
20. Ghoshal, T., Biswas, S., Nambissan, P. M. G., Majumdar, G., and De, S. K. (2009). Cadmium oxide octahedrons and nanowires on the micro-octahedrons: a simple solvothermal synthesis, *Cryst. Growth Des.*, **9**, pp. 1287–1292.
21. Yan, T., Wang, X., Long, J., Lin, H., Yuan, R., Dai, W., *et al.* (2008). Controlled preparation of In_2O_3, InOOH and $In(OH)_3$ via a one-pot aqueous solvothermal route, *New J. Chem.*, **32**, pp. 1843–1846.
22. Garnweitner, G., and Niederberger, M. (2008). Organic chemistry in inorganic nanomaterials synthesis, *J. Mater. Chem.*, **18**, pp. 1171–1182.
23. Garnweitner, G., Antonietti, M., and Niederberger, M. (2005). Nonaqueous synthesis of crystalline anatase nanoparticles in simple ketones and aldehydes as oxygen-supplying agents, *Chem. Commun.*, pp. 397–399.

24. Niederberger, M., Garnweitner, G., Buha, J., Polleux, J., Ba, J., and Pinna, N. (2006). Nonaqueous synthesis of metal oxide nanoparticles: review and indium oxide as case study for the dependence of particle morphology on precursors and solvents, *J. Sol-Gel Sci. Technol.*, **40**, pp. 259–266.
25. Pinna, N., Neri, G., Antonietti, M., and Niederberger, M. (2004). Nonaqueous synthesis of nanocrystalline semi-conducting metal oxides for gas sensing, *Angew. Chem., Int. Ed.*, **43**, p. 4345.
26. Bilecka, I., Djerdj, I., and Niederberger, M. (2008). One-minute synthesis of crystalline binary and ternary metal oxide nanoparticles, *Chem. Commun.*, pp. 886–888.
27. Djerdj, I., Arcon, D., Jaglicic, Z., and Niederberger, M. (2007). Nonaqueous synthesis of manganese oxide nanoparticles, structural characterization, and magnetic properties, *J. Phys. Chem. C*, **111**, pp. 3614–3623.
28. Nguyen, T. D., and Do, T. O. (2009). Solvo-hydrothermal approach for the shape-selective synthesis of vanadium oxide nanocrystals and their characterization, *Langmuir*, **25**, pp. 5322–5332.
29. Li, X. L., Peng, Q., Yi, J. X., Wang, X., and Li, Y. D. (2006). Near monodisperse TiO_2 nanoparticles and nanorods, *Chem. Eur. J.*, **12**, pp. 2383–2391.
30. Xie, R. C., and Shang, J. K. (2007). Morphological control in solvothermal synthesis of titanium oxide, *J. Mater. Sci.*, **42**, pp. 6583–6589.
31. Dinh, C. T., Nguyen, T. D., Kleitz, F., and Do. T. O. (2009). Shape-controlled synthesis of highly crystalline titania nanocrystals, *ACS nano*, **3**, pp. 3737–3743.
32. Zhou, Y. X., Yao, H. B., Zhang, Q., Gong, J. Y., Liu, S. J., and Yu, S. H. (2009). Hierarchical $FeWO_4$ microcrystals: solvothermal synthesis and their photocatalytic and magnetic properties, *Inorg. Chem.*, **48**, pp. 1082–1090.
33. Liang, X., Wang, X., Zhuang, Y., Xu, B., Kuang, S., and Li, Y. (2008). Formation of CeO_2–ZrO_2 solid solution nanocages with controllable structures via kirkendall effect, *J. Am. Chem. Soc.*, **130**, pp. 2736–2737.
34. Downing, E., Hesselink, L., Ralston, J., and Macfarlane, T. (1996). A three-color, solid-state, three-dimensional display, *Science*, **273**, pp. 1185–1189.
35. Gambino, J. R., and Guare, C. J. (1963). Yttrium and rare earth vanadates, *Nature*, **198**, p. 1084.
36. Boyer, J. C., Cuccia, L. A., and Capobianco, J. A. (2007). Synthesis of colloidal upconverting $NaYF_4$: Er^{3+}/Yb^{3+} and Tm^{3+}/Yb^{3+} monodisperse nanocrystals, *Nano Letter*, **7**, pp. 847–852.

37. Nguyen, T. D., Dinh, C. T., and Do, T. O. (2009). Monodisperse samarium and cerium orthovanadate nanocrystals and metal oxidation states on the nanocrystal surface, *Langmuir*, **25**, pp. 11142–11148.

38. Mullin, J. W. (1997). *Crystallization* 3rd ed. (Butterworth-Heinemann: Woburn, MA).

39. Nguyen, T. D., Dinh, C. T., and Do, T. O. (2010). Shape- and size-controlled synthesis of monoclinic ErOOH and cubic Er_2O_3 from micro- to nanostructures and their upconversion luminescence, *ACS nano*, **4**, pp. 2263–2273.

40. Brust, M., Walker, M., Bethell, D., Schiffrin, D. J., and Whyman, R. (1994). Synthesis of thiol-derivatised gold nanoparticles in a two-phase Liquid–Liquid system, *J. Chem. Soc., Chem. Commun.*, pp. 801–802.

41. Pan, D., Ji, X., An, L., and Lu, Y. (2008). Observation of nucleation and growth of CdS nanocrystals in a two-phase system, *Chem. Mater.*, **20**, pp. 3560–3566.

42. Wang, Q., Pan, D. C., Jiang, S. C., Ji, X. L., An, L. J., and Jiang, B. Z. (2005). A new two-phase route to high-quality CdS nanocrystals, *Chem. Eur. J.*, **11**, pp. 3843–3848.

43. Pan, D. C., Jiang, S. C., An, L. J., and Jiang, B. Z. (2004). Controllable synthesis of highly luminescent and monodisperse CdS nanocrystals by a two-phase approach under mild conditions, *Adv. Mater.*, **16**, pp. 982–985.

44. Pan, D. C., Zhao, N. N., Wang, Q., Jiang, S. C., Ji, X. L., and An, L. J. (2005). Facile synthesis and characterization of luminescent TiO_2 nanocrystals, *Adv. Mater.*, **17**, pp. 1991–1995.

45. Zhao, N. N., Pan, D. C., Nie, W., and Ji, X. L. (2006). Two-phase synthesis of shape-controlled colloidal zirconia nanocrystals and their characterization, *J. Am. Chem. Soc.*, **128**, pp. 10118–10124.

46. Du, H., Wohlrab, S., Weiss, M., and Kaskel, S. (2007). Preparation of $BaTiO_3$ nanocrystals using a two-phase solvothermal method, *J. Mater. Chem.*, **17**, pp. 4605–4610.

47. Zhang, J., Ohara, S., Umetsu, M., Naka, T., Hatakeyama, Y., and Adschiri, T. (2007). Colloidal ceria nanocrystals: a tailor-made crystal morphology in supercritical water, *Adv. Mater.*, **19**, pp. 203–206.

48. Zhao, N. N., Nie, W., Liu, X. B., Tian, S. Z., Zhang, Y., and Ji, X. L. (2008). Shape- and size-controlled synthesis and dependent magnetic properties of nearly monodisperse Mn_3O_4 nanocrystals, *Small*, **4**, pp. 77–81.

49. Mrabet, D., Zahedi-Niaki, M. H., and Do, T. O. (2008). Synthesis of nanoporous network materials with high surface areas from the cooperative assemblage of alkyl-chain-capped metal/metal oxide nanoparticles, *J. Phys. Chem. C*, **112**, pp. 7124–7129.
50. Nguyen, T. D., and Do, T. O. (2009). General two-phase routes to synthesize colloidal metal oxide nanocrystals: simple synthesis and ordered self-assembly structures, *J. Phys. Chem. C*, **113**, pp. 11204–11214.
51. Murray, C. B., Norris, D. J., and Bawendi, M. G. (1993). Synthesis and characterization of nearly monodisperse CdE (E = sulfur, selenium, tellurium) semiconductor nanocrystallites, *J. Am. Chem. Soc.*, **115**, pp. 8706–8715.
52. Peng, X., Wickham, J., and Alivisatos, A. P. (1998). Kinetics of II-VI and III-V colloidal semiconductor nanocrystal growth: "focusing" of size distributions, *J. Am. Chem. Soc.*, **120**, pp. 5343–5344.
53. O'Brien, S., Brus, L., and Murray, C. B. (2001). Synthesis of monodisperse nanoparticles of barium titanate: toward a generalized strategy of oxide nanoparticle synthesis, *J. Am. Chem. Soc.*, **123**, pp. 12085–12086.
54. Park, J., Joo, J., Kwon, S. G., Jang, Y., and Hyeon, T. (2007). Synthesis of monodisperse spherical nanocrystals, *Angew. Chem. Int. Ed.*, **46**, pp. 4630–4660.
55. Shevchenko, E. V., Talapin, D. V., Murray, C. B., and O'Brien, S. (2006). Structural characterization of self-assembled multifunctional binary nanoparticle superlattices, *J. Am. Chem. Soc.*, **128**, pp. 3620–3637.
56. Hyeon, T., Lee, S. S., Park, J., Chung, Y., and Na, H. B. (2001). Synthesis of highly crystalline and monodisperse maghemite nanocrystallites without a size-selection process, *J. Am. Chem. Soc.*, **123**, pp. 12798–12801.
57. Park, J., Kang, E., Bae, C. J., Park, J. G., Noh, H. J., Kim, J. Y., *et al.* (2004). Synthesis, characterization, and magnetic properties of uniform-sized MnO nanospheres and nanorods, *J. Phys. Chem. B*, **108**, pp. 13594–13598.
58. Park, J., Lee, E., Hwang, N. M., Kang, M., Kim, S. C., Hwang, Y., *et al.* (2005). One-nanometer-scale size-controlled synthesis of monodisperse magnetic iron oxide nanoparticles, *Angew. Chem., Int. Ed.*, **44**, pp. 2872–2877.
59. Lee, K., Seo, W. S., and Park, J. T. (2003). Synthesis and optical properties of colloidal tungsten oxide nanorods, *J. Am. Chem. Soc.*, **125**, pp. 3408–3409.
60. Park, J. C., and Song, H. (2007). Synthesis of polycrystalline Mo/MoO_x nanoflakes and their transformation to MoO_3 and MoS_2 nanoparticles, *Chem. Mater.*, **19**, pp. 2706–2708.

61. Kang, E., Park, J., Hwang, Y., Kang, M., Park, J. G., and Hyeon, T. (2004). Direct synthesis of highly crystalline and monodisperse manganese ferrite nanocrystals, *J. Phys. Chem. B*, **108**, pp. 13932–13935.

62. Niederberger, M., and Garnweitner, G. (2006). Organic reaction pathways in the nonaqueous synthesis of metal oxide nanoparticles, *Chem. Eur. J.*, **12**, pp. 7282–7302.

63. Willis, A. L., Chen, Z., He, J., Zhu, Y., Turro, N. J., and O'Brien, S. (2007). Metal acetylacetonates as general precursors for the synthesis of early transition metal oxide nanomaterials, *J. Nanomater.*, Article ID 14858, 7 pages (doi:10.1155/2007/14858).

64. Kim, D., Lee, N., Park, M., Kim, B. H., An, K., and Hyeon, T. (2009). Synthesis of uniform ferrimagnetic magnetite nanocubes, *J. Am. Chem. Soc.*, **131**, pp. 454–455.

65. Song, Q., and Zhang, Z. J. (2004). Shape control and associated magnetic properties of spinel cobalt ferrite nanocrystals, *J. Am. Chem. Soc.*, **126**, pp. 6164–6168.

66. Cao, Y. C. (2004). Synthesis of square gadolinium-oxide nanoplates, *J. Am. Chem. Soc.*, **126**, pp. 7456–7457.

67. Yu, T., Joo, J., Park, Y. I., and Hyeon, T. (2006). Single unit cell thick samaria nanowires and nanoplates, *J. Am. Chem. Soc.*, **128**, pp. 1786–1787.

68. Yu, T., Moon, J., Park, J., Park, Y. I., Na, H. B., Kim, B. H., *et al.* (2009). Various-shaped uniform Mn_3O_4 nanocrystals synthesized at low temperature in air atmosphere, *Chem. Mater.*, **21**, pp. 2272–2279.

69. Jana, N. R., Chen, Y., and Peng, X. (2004). Size- and shape-controlled magnetic (Cr, Mn, Fe, Co, Ni) oxide nanocrystals via a simple and general approach, *Chem. Mater.*, **16**, pp. 3931–3935.

70. Albertina, C., and Martyn, P. (2001). The continuous hydrothermal synthesis of nano-particulate ferrites in near critical and supercritical water, *J. Mater. Chem.*, **11**, pp. 1408–1416.

71. Si, R., Zhang, Y. W., You, L. P., and Yan, C. H. (2005). Rare-earth oxide nanopolyhedra, nanoplates, and nanodisks, *Angew. Chem.*, **117**, pp. 3320–3324.

72. Cozzoli, P. D., Kornowski, A., and Weller, H. (2003). Low-temperature synthesis of soluble and processable organic-capped anatase TiO_2 nanorods, *J. Am. Chem. Soc.*, **125**, pp. 14539–14548.

73. Seo, J., Jun, Y., Ko, S. J., and Cheon, J. (2005). *In situ* one-pot synthesis of 1-dimensional transition metal oxide nanocrystals, *J. Phys. Chem. B*, **109**, pp. 5389–5391.

74. Park, J., An, K., Hwang, Y., Park, J. G., Noh, H. J., Kim, J. Y., *et al*. (2003). Ultra-large-scale synthesis of monodisperse nanocrystals, *Nature Mater*., **3**, pp. 891–895.

75. An, K., Kwon, S. G., Park, M., Na, H. B., Baik, S. I., Yu, J. H., *et al*. (2008). Synthesis of uniform hollow oxide nanoparticles through nanoscale acid etching, *Nano Lett*., **8**, pp. 4252–4258.

76. Langevin, D. (1992). Micelles and microemulsions, *Annu*. *Rev*. *Phys*. *Chem*., **43**, pp. 341–369.

77. Paul, B. K., and Moulik, S. P. (2001). Uses and applications of microemulsions, *Curr*. *Sci*., **80**, pp. 990–1001.

78. Gutmann, H., and Kertes, A. S. (1975). Cationic surfactants in organic solvents III. Critical micelle concentration of dodecylammonium halides in benzene and toluene, *J*. *Colloid Interface Sci*., **51**, pp. 406–411.

79. Capek, I. (2004). Preparation of metal nanoparticles in water-in-oil (w/o) microemulsions, *Adv*. *Colloid Interface Sci*., **110**, pp. 49–74.

80. Kuiry, S. C., Patil, S. D., Deshpande, S., and Seal, S. (2005). Spontaneous self-assembly of cerium oxide nanoparticles to nanorods through supraaggregate formation, *J*. *Phys*. *Chem*. *B*, **109**, pp. 6936–6939.

81. Bai, F., Wang, D., Huo, Z., Chen, W., Liu, L., Liang, X., *et al*. (2007). A versatile bottom-up assembly approach to colloidal spheres from nanocrystals, *Angew*. *Chem*., **119**, pp. 6770–6773.

82. Li, M., Schmablegger, H., and Mann, S. (1999). Coupled synthesis and self-assembly of nanoparticles to give structures with controlled organization, *Nature*, **402**, pp. 393–395.

83. Johnson, C. J., Li., M., and Mann, S. (2004). Seed-assisted synthesis of $BaCrO_4$ nanoparticles and nanostructures in water-in-oil microemulsions, *Adv*. *Funct*. *Mater*., **14**, pp. 1233–1239.

84. Kim, F., Kwan, S., Akana, J., and Yang, P. (2001). Langmuir–blodgett nanorod Assembly, *J*. *Am*. *Chem*. *Soc*., **123**, pp. 4360–4361.

85. Cozzoli, P. D., and Manna, L. (2007). Synthetic strategies to size and shape controlled nanocrystals and nanocrystal heterostructures, in *Bio-Application of Nanoparticles* (Chan, W. C. W., Ed.), Landes Bioscience and Springer Science+Business Media, pp. 1–17.

86. Zhang, J., Huang, F., and Lin, Z. (2010). Progress of nanocrystaline growth kinetics based on oriented attachment, *Nanoscale*, **2**, pp. 18–34.

87. Penn, R. L., and Banfield, J. F. (1999). Morphology development and crystal growth in nanocrystalline aggregates under hydrothermal conditions: insights from titania, *Geochim*. *Cosmochim*. *Acta*, **63**, pp. 1549–1557.

88. Pacholski, C., Kornowski, A., and Weller, H. (2002). Self-assembly of ZnO: from nanodots to nanorods, *Angew. Chem. Int. Ed.*, **41**, pp. 1188–1191.

89. Zitoun, D., Pinna, N., Frolet, N., and Belin, C. (2005). Single crystal manganese oxide multipods by oriented attachment, *J. Am. Chem. Soc.*, **127**, pp. 15034–15035.

90. Nguyen, T. D., Mrabet, D., and Do, T. O. (2008). Controlled self-assembly of Sm_2O_3 nanoparticles into nanorods: simple and large scale synthesis using bulk Sm_2O_3 powders, *J. Phys. Chem. C*, **112**, pp. 15226–15235.

91. Venables, J. A. (2000). *Introduction to Surface and Thin Film Processes* (Cambridge University Press, Cambridge).

92. Peng, X., Manna, L., Yang, W., Wickham, J., Scher, E., Kadavanich, A., *et al.* (2000). Shape control of CdSe nanocrystals, *Nature*, **404**, pp. 59–61.

93. Jun, Y., Casula, F., Sim, J.-H., Kim, S. Y., Cheon, J., and Alivisatos, A. P. (2003). Surfactant-assisted elimination of a high energy facet as a means of controlling the shapes of TiO_2 nanocrystals, *J. Am. Chem. Soc.*, **125**, pp. 15981–15985.

94. Peng, Z. A., and Peng, X. (2001). Mechanisms of the shape evolution of CdSe nanocrystals, *J. Am. Chem. Soc.*, **123**, pp. 1389–1395.

95. Lee, S.-M., Jun, Y.-W., Cho, S.-N., and Cheon, J. (2002). Single-crystalline star-shaped nanocrystals and their evolution: programming the geometry of nano-building blocks, *J. Am. Chem. Soc.*, **124**, pp. 11244–11245.

96. Feng, X., Sayle, D. C., Wang, Z. L., Paras, M. S., Santora, B., Sutorik, A. C., *et al.* (2006). Converting ceria polyhedral nanoparticles into single-crystal nanospheres, *Science*, **312**, pp. 1504–1508.

97. Farvid, S. S., Dave, N., Wang, T., and Radovanovic, P. V. (2009). Dopant-induced manipulation of the growth and structural metastability of colloidal indium oxide nanocrystals, *J. Phys. Chem. C*, **113**, pp. 15928–15933.

98. Wang, F., Han, Y., Lim, C. S., Lu, Y., Wang, J., Xu, J., *et al.* (2010). Simultaneous phase and size control of upconversion nanocrystals through lanthanide doping, *Nature*, **463**, pp. 1061–1065.

99. Chen, D., Yu, Y., Huang, F., Huang, P., Yang, A., and Wang, Y. (2010). Modifying the size and shape of monodisperse bifunctional alkaline-earth fluoride nanocrystals through lanthanide doping, *J. Am.Chem. Soc.*, **132**, pp. 9976–9978.

100. Yang, Y., Jin, Y., He, H., Wang, Q., Tu, Q., Lu, H., *et al.* (2010). Dopant-induced shape evolution of colloidal nanocrystals: the case of zinc oxide, *J. Am. Chem. Soc.*, **132**, pp. 13381–13394.

101. Lu, A. H., and Schüth, F. (2006). Nanocasting: a versatile strategy for creating nanostructured porous materials, *Adv*. *Mater*., **18**, pp. 1793–1805.

102. Lu, A. H., Zhao, D., and Wan, Y. (2010). *Nanocasting — A versatile strategy for creating nanostructured porous materials* (RSC publishing).

103. Salabas, E. L., Rumplecker, A., Kleitz, F., Radu, F., and Schüth, F. (2006). Exchange anisotropy in nanocasted Co_3O_4 nanowires, *Nano Lett*. **6**, pp. 2977–2981.

104. Rumplecker, A., Kleitz, F., Salabas, E. L., and Schüth, F. (2007). Hard templating pathway for the synthesis of nanostructured porous Co_3O_4, *Chem*. *Mater*., **19**, pp. 485–496.